Nonuniform transformation field analysis of materials with morphological anisotropy

F. Fritzen, T. Böhlke

Nonuniform transformation field analysis of materials with morphological anisotropy

F. Fritzen, T. Böhlke

PII: S0266-3538(10)00481-1
DOI: 10.1016/j.compscitech.2010.12.013
Reference: CSTE 4878

To appear in: *Composites Science and Technology*

Received Date: 25 June 2010
Revised Date: 6 December 2010
Accepted Date: 12 December 2010

Please cite this article as: Fritzen, F., Böhlke, T., Nonuniform transformation field analysis of materials with morphological anisotropy, *Composites Science and Technology* (2010), doi: 10.1016/j.compscitech.2010.12.013

Nonuniform transformation field analysis of materials with morphological anisotropy

F. Fritzen, T. Böhlke

Chair for Continuum Mechanics, Institute of Engineering Mechanics, Karlsruhe Institute of Technology, Kaiserstr. 10, building 10.23, 3rd floor, D-76131 Karlsruhe, Germany

Abstract. The effective properties of metal matrix composites with particulate reinforcement are investigated using the nonuniform transformation field analysis (NTFA) developed by Michel and Suquet (2003). In particular the effect of the particle morphology on the effective mechanical response is examined in detail. For that, an existing periodic three-dimensional mesh generation technique for particulate composites is extended to allow for anisotropic morphologies. It is shown that the effects induced by the anisotropic particles can be captured by the NTFA. Additionally, the load partitioning between reinforcement and matrix material is investigated and a good agreement to full-field computations is attained with the NTFA.

Keywords: Multiscale modeling Metal-matrix composites (MMCs) Non-linear behaviour Anisotropy Finite element analysis (FEA)

1. Introduction

Composite materials based on particle, whisker and short fiber reinforcements form the basis for the design of many structures in, e.g., vehicle, ship and aerospace industry (Suresh, S., 2002; Miracle, 2005). For these engineering applications the mechanical properties of the composites are much sought after quantities, i.e., for the use in finite element simulations. Due to high experimental costs, a need for tools that allow for an efficient numerical prediction of the mechanical behaviour of composites emerges.

The estimation of the mechanical properties of micro-heterogeneous materials is a well-established field of research for many years. Simple approaches are based on simple mixtures theories, i.e., upper (Voigt, 1910) and lower (Reuss, 1929) estimates or the singular approximation (Böhlke et al., 2010). A more refined approach was developed by Hashin and Shtrikman (1962) and generalized by Willis (1977) to provide narrower upper and lower estimates. Based on the Eshelby solution for an ellipsoidal inclusion, efficient algorithms for the prediction of the linear properties of particulate structures with near isotropic inclusions were found by Mori and Tanaka (1973). Self-consistent estimates (Kröner, 1958) were developed, which overpredict the stiffness of the particle reinforcement systems with high phase contrast (see, e.g., Fritzen and Böhlke (2010b)). All these methods rely on the linearity of the material response. Consequently, non-linear behavior induced by plasticity can usually not be included in the mentioned methods

without additional considerations, see, e.g., Doghri and Ouaar (2003).

With the increase in the computational performance and the number of available numerical software products, computational homogenization methods have gained importance. In these methods the local constitutive behavior is fully resolved and the physically non-linear problem is solved numerically. Based on the attained microscopic solution and an averaging procedure the effective or apparent response of the micro-heterogeneous material is determined (see, e.g., Kanoute et al., 2009). An interesting concept was developed by Ghosh et al. (1995, 1996) (and follow-ups) in terms of a special class of finite element based on Voronoi cells. These special elements have a large number of degrees of freedom and incorporate an ellipsoidal inclusion, i.e., they are limited to particulate materials with near ellipsoidal shape.

A promising approach towards a more general micro-mechanical homogenization method is the transformation field analysis (TFA) introduced by Dvorak and Benveniste (1992). It links analytical and computational approaches by a computational evaluation of the localization operators. The main conceptual point is the replacement of the plastic strain field by piecewise constant fields. Thereby, a set of reduced constitutive relations for the heterogeneous material can be derived which leads to a massive reduction in the number of degrees of freedom. Due to its micro-mechanical motivation and its rather straight-forward formulation the method has been applied and extended in the past two decades (see, e.g., Dvorak and Zhang, 2001; Carrere et al., 2003; Chaboche et al., 2005; Oskay and Fish, 2007).

The non-uniform transformation field analysis primarily developed by Michel and Suquet (2003, 2004) and extended by Roussette et al. (2009) is a computational homogenization method based on a micro-mechanical concept. In contrast to the TFA which it is based on, the NTFA allows for a parametrization of the inelastic strain using spatially nonuniform plastic strain fields, the so called inelastic modes. The method has been shown to be a very efficient tool for the homogenization of the inelastic material properties of micro-heterogeneous materials with two-dimensional microstructure. The considered materials were either orthotropic or hexagonal (single fiber models) or statistically almost isotropic (multi-fiber models). Recently, the authors have rewritten the basic equations of the NTFA (Fritzen and Böhlke, 2010c) and discussed details concerning the numerical implementation. Particular emphasis was placed on the finite element based mode identification and the structural application of the homogenized material model. The authors found an excellent agreement between full-field simulations and the reduced model for quasi-isotropic particle reinforced composites in a fully three-dimensional context (Fritzen and Böhlke, 2009a,b; Fritzen and Böhlke, 2010c). Simultaneously, Michel and Suquet (2009) have applied the NTFA in combination with a finite element based mode identification procedure to a two-dimensional bi-material with hexagonal sub-structure with success. In the latter work the class of constitutive models was extended to allow for non-linear kinematic hardening. In all of the prior studies the examined microstructures were statistically almost isotropic, or single fiber models were used. However, in many real materials the microstructure is intrinsically anisotropic. For instance, it was found by Ganesh and Chawla (2005) that Al/SiC_p composites produced in an extrusion process show a morphological anisotropy that influences the elastic and inelastic

material properties of the composite.

The treatment of the morphological anisotropy of micro-heterogeneous materials with particle reinforcement is the focus of this contribution. Therefore, a modification of the mesh generation technique developed by Fritzen and Böhlke (2010b) is presented in section 2 in order to account for a class of morphological anisotropy. The generated model microstructures are used in combination with the non-uniform transformation field analysis briefly revisited in section 3 to generate reduced constitutive equations for the microstructured material on the macroscopic scale. Anisotropic elastic effects resulting from the particle shape are discussed in section 4. The NTFA is then applied to investigate the inelastic material behavior of the composite. The effective stress tensor predicted by the homogenized material model involving a small number of internal variables is compared to results obtained from full-field simulations based on several hundred thousand degrees of freedom. Furthermore, the load transfer between the matrix material and the ceramic constituent is investigated based on the NTFA for the different particle shapes. The paper closes with a summary.

2. Periodic mesh generation for anisotropic model microstructures

Based on an algorithm for the generation of periodic unstructured meshes for polycrystalline aggregates (Fritzen et al., 2009), the authors have recently proposed an extension for particle reinforced composites (Fritzen and Böhlke, 2010b). The generated model microstructures are based on the Voronoi tessellation and allow for arbitrary particle volume fractions. The latter is a difference with respect to other approaches, e.g., Flaquer et al. (2007), which can only attain high volume fractions when employing additional techniques such as simulated annealing.

While the method presented in (Fritzen and Böhlke, 2010b) is suitable for the description of near isotropic materials, some materials exhibit a pronounced morphological anisotropy. The latter is, e.g., caused by an extrusion or rolling processes during the production of the composite material. The thereby introduced anisotropy can often be characterized in terms of a average deformation gradient $\bar{\boldsymbol{F}}$ (Jöchen et al., 2010). In order to account for a possible morphological anisotropy of the particles, our approach is as follows (step numbers refer to Fig. 1):

- Generate a random Voronoi tessellation based on a random point seed (steps 1 & 2) (the point seed can possibly be constrained, see, e.g. Du et al. (1999)). The fast and robust `qhull` library is employed (Barber et al., 1996).
- Deform the generated tessellation (step 3) based on the tensorial morphological anisotropy $\bar{\boldsymbol{F}}$ by updating all cell corner points $\boldsymbol{x}_i$ according to the affine transformation ($\lambda_1, \lambda_2 > 0$)

$$\boldsymbol{x}_i \rightarrow \bar{\boldsymbol{F}}\boldsymbol{x}_i, \qquad \bar{\boldsymbol{F}} = \begin{pmatrix} \lambda_1 & & \\ & \lambda_2 & \\ & & (\lambda_1\lambda_2)^{-1} \end{pmatrix} \boldsymbol{e}_i \otimes \boldsymbol{e}_j. \tag{1}$$

  Note that the geometry is modified *before* the mesh is generated. This allows for the creation of a high quality spatial discretization on the deformed geometry with (almost) isotropic

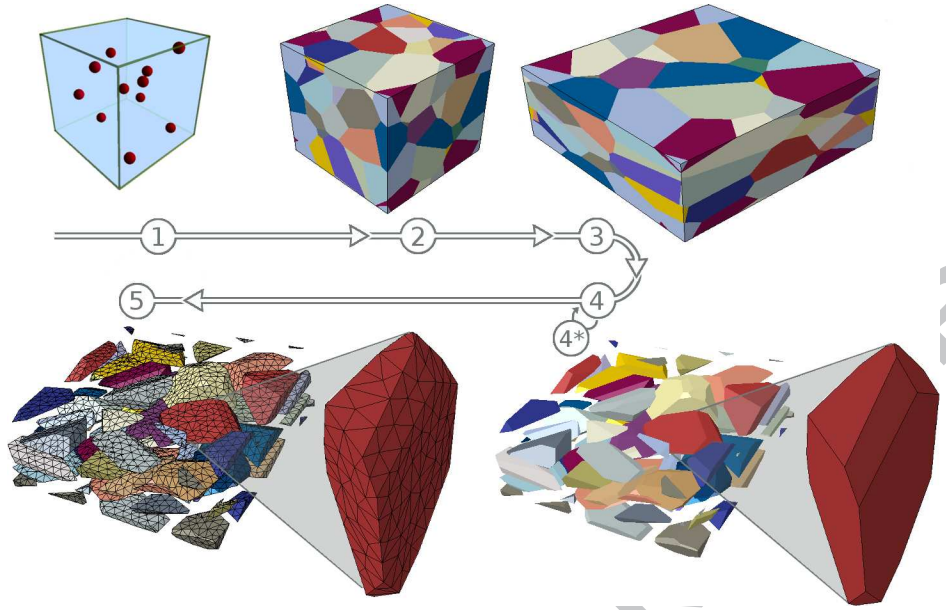

Fig. 1: Flow diagram for the generation of the model microstructures including the periodic mesh generation

element shapes. Additionally, the periodicity of the model microstructure is invariant under the affine transformation (1).

- Shrink the cells according to the algorithm presented in Fritzen and Böhlke (2010b) (step 4) and iterate the cell wall thickness until the desired volume fraction is reached (optional: step 4*).

- Generate a periodic volume mesh based on the generated particle geometry (step 5) using the hierarchical mesh generation algorithm used by Fritzen et al. (2009); Fritzen and Böhlke (2010b). The libraries `triangle` (Shewchuk, 1996) and `tetgen` (Si and Gaertner, 2005) are used.

The average particle shape resulting from the original Voronoi tessellation is isotropic, i.e. can be represented in terms of a sphere (Fig. 2 middle, top). Denote that individual realizations of the particles may, however, be non-isotropic as can be seen from the two depicted particles. Two classed of morphological anisotropies are considered in this work

- Oblate particles (Fig. 2, left) with

$$\bar{\boldsymbol{F}} = \begin{pmatrix} \lambda^{-1} & & \\ & \sqrt{\lambda} & \\ & & \sqrt{\lambda} \end{pmatrix} \boldsymbol{e}_i \otimes \boldsymbol{e}_j, \qquad \lambda > 1, \tag{2}$$

- Elongated particles (Fig. 2, right) with

$$\bar{\boldsymbol{F}} = \begin{pmatrix} \lambda & & \\ & \lambda^{-1/2} & \\ & & \lambda^{-1/2} \end{pmatrix} \boldsymbol{e}_i \otimes \boldsymbol{e}_j, \qquad \lambda > 1. \tag{3}$$

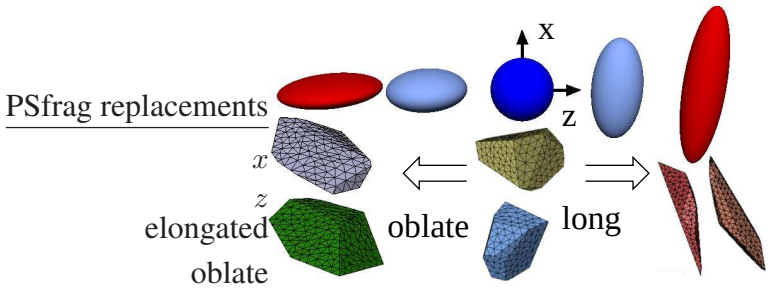

Fig. 2: Variations of the shape of idealized particles (top) and realizations of individual particles (bottom); values for λ are 2.25, 1.5625, 1 (sphere), 1.5625, 2.56 (left to right)

Some example meshes are presented in Fig. 3 for oblate particles ($\lambda = 2, 4$) and in Fig. 4 for elongated particles ($\lambda = 2, 4$). The anisotropy of the particle shape can be described by means of the aspect ratio

$$\eta = \lambda^{3/2} \tag{4}$$

of the principle axes of the idealized particle for the two morphological modifications. The following investigations are based on the values $\lambda \in \{2, 3, 4\}$.

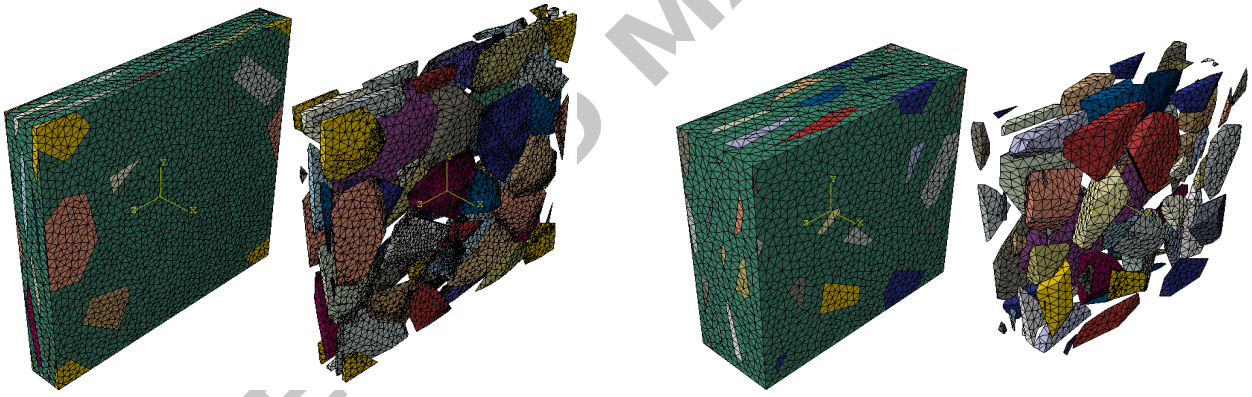

Fig. 3: Periodic mesh of unit cells containing 40 oblate particles for $\lambda = 2, 4$ (left to right); meshes consist of 102000 ($\lambda = 2$) and 141000 ($\lambda = 4$) nodes respectively

Note that the aspect ratio of the particles for $\lambda = 4$ is $\eta = 8$, i.e. a high aspect ratio is attained. The number of particles was set to 40 and a volume fraction of 20 % was decided on. The mesh density in the simulations varied between 300000-425000 degrees of freedom depending on the value of λ. In order to compare the elastic and inelastic properties of the anisotropic particle composites to a reference structure, an isotropic particle distribution, i.e. $\lambda = 1$, was also considered. The mesh density and the particle volume fraction and the number of degrees of freedom were chosen according to the other microstructures.

The geometrical properties of the particles are studied in terms of the minimum feret $d_i^{\min}$ and the maximum feret $d_i^{\max}$ of the i-th particle, see also Fig. 5. The corresponding principle axis have also been analyzed. Their distribution is exemplified in Fig. 6 for the isotropic material (left), the elongated microstructure ($\lambda = 4$, middle) and the oblate microstructure ($\lambda = 4$, right). The

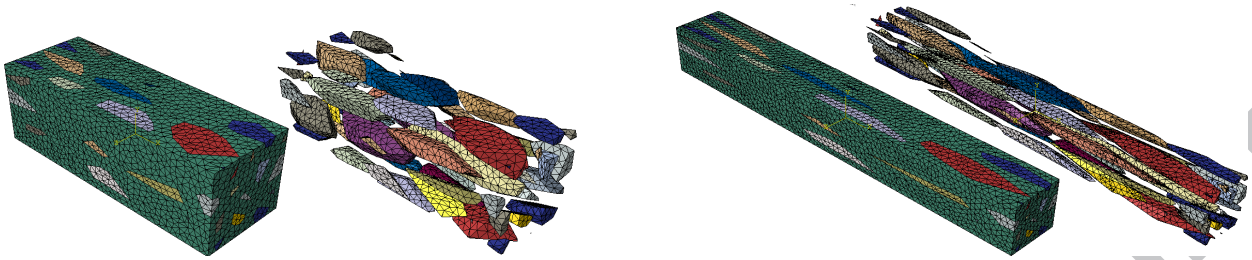

Fig. 4: Periodic mesh of unit cells containing 40 elongated particles for $\lambda = 2, 4$ (left to right); meshes consist of 101000 ($\lambda = 2$) and 120000 ($\lambda = 4$) nodes respectively

directions representing the smallest particle elongation $\boldsymbol{n}_i^{\min}$ and the largest particle elongation $\boldsymbol{n}_i^{\max}$ are drawn for each of the 40 inclusions for each of the three microstructures. It can be concluded that the distribution of the principle axis follows the imposed macroscopic deformation. For the two anisotropic microstructures the directors are distributed isotropic in the y-z-plane.

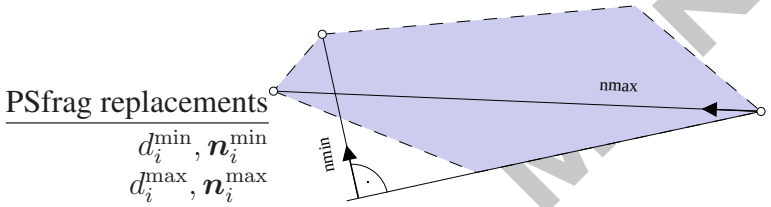

Fig. 5: Minimum and maximum feret of a convex particle

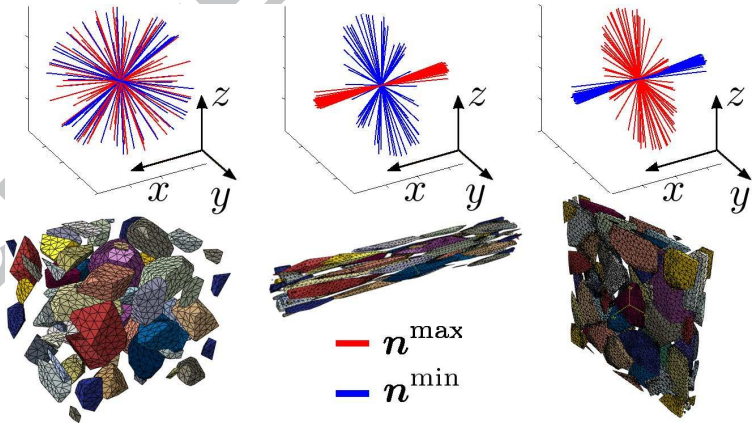

Fig. 6: Directions of the minimum and maximum feret for three microstructures; drawn are the directors $\boldsymbol{n}_i^{\min}, \boldsymbol{n}_i^{\max}$ for all 40 particles

In addition the anisotropy of the particles was analysed by taking the mean aspect ratio. The latter is defined via the grain elongations l_x, l_y, l_z with respect to the orthonormal coordinate axis. For

the oblate and elongated microstructures we define the mean anisotropy via

$$\mathcal{A}_{\mathrm{o}} = \frac{1}{N}\sum_{i=1}^{N}\frac{l_{y,i}+l_{z,i}}{2l_{x,i}}, \qquad \mathcal{A}_{\mathrm{e}} = \frac{1}{N}\sum_{i=1}^{N}\frac{2l_{x,i}}{l_{y,i}+l_{z,i}}. \tag{5}$$

The results are shown in Tab. 1. The results confirm that the anisotropy of the particles is significant even for $\lambda = 2$.

	oblate				elongated		
λ	2	3	4	λ	2	3	4
$\mathcal{A}_{\mathrm{o}}$	3.852	7.639	11.581	$\mathcal{A}_{\mathrm{e}}$	3.343	6.338	9.849

Table 1: Average particle aspect ratios for the oblate and the elongated microstructures

Additionally, the properties of the Al/SiC material examined by Ganesh and Chawla (2005) have been replicated. In order to do so, a set of parameters has been identified and the aspect ratios of the particles of the artificial material are compared to the values given in Ganesh and Chawla (2005), Tab. 1 for 20% particle volume fraction. The longitudinal and transversal particle aspect ratios $\mathcal{R}_{\mathrm{L}}$ and $\mathcal{R}_{\mathrm{T}}$ for the artificial composite material are

$$\mathcal{R}_{\mathrm{L}} = 2.2554 \pm 0.7304, \qquad \mathcal{R}_{\mathrm{T}} = 2.0915 \pm 0.8365. \tag{6}$$

By comparison to the values provided by Ganesh and Chawla the model microstructures can be considered suitable to replicate real materials with anisotropic particle shape to a considerable extent. While the mean aspect ratio is almost exactly replicated, the standard deviation is slightly underestimated.

All finite element calculations are carried out using quadratic tetrahedral elements and periodic displacement fluctuation boundary conditions. The latter are massively superior to uniform traction or displacement boundary conditions for the considered class of unit cell problems. This is due to the fact that the surface of the unit cell and, hence, the number of boundary nodes is large. In the case of homogeneous displacement constraints a boundary close region of influence is induced in which the results can merely help to predict the *true* effective response of the composite. Consequently, one would have to massively increase the size of the unit cell (i.e., the number of particles) in order to attain only minor boundary effects and, thereby, the number of degrees of freedom.

3. Framework of the non-uniform transformation field analysis

In the following a mechanical two scale problem (Fig. 7) is examined, where the scales are assumed to be separated (e.g., Willis (1981)). Particularly, it is assumed that the *fastest* fluctuation (with respect to the spatial coordinate) of a field on the macroscopic (structural) level is *small* with respect to the length of the unit cell. The often formulated condition

$$L \gg l \tag{7}$$

with L the length of the macroscopic problem and l the size of the unit cell is not sufficient for a scale separation in general. Fields existing on both scales, i.e. the displacement $\boldsymbol{u}$, Cauchy's stress tensor $\boldsymbol{\sigma}$ and the infinitesimal strain tensor $\boldsymbol{\varepsilon}$, live on the microscale or, if over-lined, on the macroscopic scale. For example $\boldsymbol{\sigma}$ denotes the micro stress and $\bar{\boldsymbol{\sigma}}$ denotes the stress tensor on the macroscopic level. The stress and strain fields on both scales are related by

$$\bar{\boldsymbol{\sigma}} = \langle \boldsymbol{\sigma} \rangle, \qquad \bar{\boldsymbol{\varepsilon}} = \langle \boldsymbol{\varepsilon} \rangle, \tag{8}$$

where $\langle \bullet \rangle$ denotes the averaging operator on the unit cell. The small strain framework is used on both scales. Then the symmetric gradient of the displacement field constitutes the strain tensor $\boldsymbol{\varepsilon}$ and the total strain is additively decomposed into an elastic part $\boldsymbol{\varepsilon}^{\mathrm{e}}$ and a plastic part $\boldsymbol{\varepsilon}^{\mathrm{p}}$.

PStrag replacements

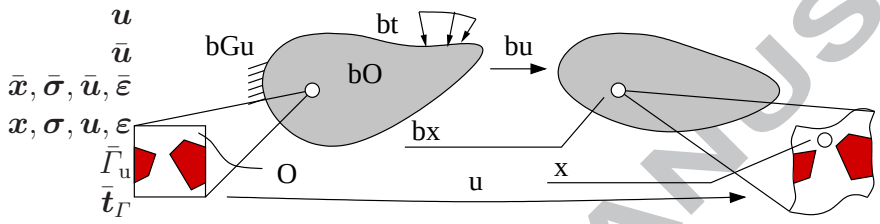

Fig. 7: Macroscopic (structural) problem and associated microscopic problem

The macroscopic and microscopic problem in the considered setting read

$$\operatorname{div}(\bar{\boldsymbol{\sigma}}) + \bar{\varrho}\bar{\boldsymbol{b}} = \boldsymbol{0}, \qquad \bar{\boldsymbol{u}} = \bar{\boldsymbol{u}}_{\Gamma} \text{ on } \bar{\Gamma}_{\mathrm{u}}, \qquad \bar{\boldsymbol{\sigma}}\bar{\boldsymbol{n}} = \boldsymbol{t}_{\Gamma} \text{ on } \bar{\Gamma}_{\mathrm{t}}, \tag{9}$$

$$\operatorname{div}(\boldsymbol{\sigma}) = \boldsymbol{0}, \qquad \langle \boldsymbol{\varepsilon} \rangle = \bar{\boldsymbol{\varepsilon}}, \qquad \boldsymbol{\sigma} \text{ is admissible.} \tag{10}$$

For rate-independent plasticity the admissibility of $\boldsymbol{\sigma}$ on the microscale is often described by some sort of yield function $\varphi(\boldsymbol{\sigma})$, which has to satisfy $\varphi \leq 0$ for any admissible state. As mentioned earlier, periodic displacement fluctuation conditions are assumed, which is an additional, noteworthy, constitutive assumption. However, the theory presented in the following is not restricted to the periodicity of the fluctuation fields, as was already pointed out in Fritzen and Böhlke (2010c).

The homogenization of the constitutive behavior of physically non-linear materials under arbitrary loading is generally hindered by the unknown structure of the constitutive equations on the structural level. For the class of generalized standard materials (GSM, Halphen and Nguyen (1975)) it is known, e.g., from the work of Suquet (1985) that the GSM structure is preserved upon transition of scales. Unfortunately, the number of internal variables is infinite for the macroscopic problem. In order to overcome this short-coming, Dvorak et al. (1994a,b) has separated the individual components into subdomains with piecewise uniform inelastic strain. Thereby, a finite number of internal variables was recovered and the transformation field analysis (TFA) was initiated. While the TFA can yield good results for some problems, the intrinsic non-uniformity of the inelastic strain field cannot be captured. Moreover, a precise prediction of the macroscopic response requires a substantial number of subdomains and is, therefore, computationally expensive. Notably, the choice of the subdomains is not a straight forward

procedure and highly influences the computational results.

In order to capture the non-uniformity of the inelastic strain field Michel and Suquet (2003, 2004) proposed to use N non-uniform basis functions $\boldsymbol{\mu}_\alpha(\boldsymbol{x})$ to parametrize the inelastic strain $\boldsymbol{\varepsilon}^{\mathrm{p}}(t,\boldsymbol{x})$ according to

$$\boldsymbol{\varepsilon}^{\mathrm{p}}(t,\boldsymbol{x}) = \sum_{\alpha=1}^{N} \xi_\alpha(t)\boldsymbol{\mu}_\alpha(\boldsymbol{x}). \tag{11}$$

Particularly, the dependency of the plastic deformation with respect to space-time is separated into time-invariant, but spatially non-uniform inelastic modes $\boldsymbol{\mu}_\alpha$ and time-dependent scalars ξ_α. In the following we refer to ξ_α as mode stimulation coefficients. The modified mode restrictions of Michel and Suquet (2003) proposed in Fritzen and Böhlke (2010c)

$$\langle \|\boldsymbol{\mu}\|_2 \rangle_{\Omega_p} = 1, \qquad \mathrm{tr}(\boldsymbol{\mu}_\alpha) = 0, \qquad \langle \boldsymbol{\mu}_\alpha \cdot \boldsymbol{\mu}_\beta \rangle = 0 \quad (\alpha \neq \beta) \tag{12}$$

are employed and the modes are chosen according to the proposal of Roussette et al. (2009) based on the Karhunen-Loève decomposition. Each inelastic mode $\boldsymbol{\mu}_\alpha$ is considered in an eigenstress problem of the form

$$\mathrm{div}(\mathbb{C}[\boldsymbol{\varepsilon}^*_\alpha - \boldsymbol{\mu}_\alpha]) = \boldsymbol{0}, \qquad \langle \boldsymbol{\varepsilon}^*_\alpha \rangle = \boldsymbol{0}, \tag{13}$$

with the elastic fourth-order stiffness tensor $\mathbb{C}$. The solution $\boldsymbol{u}^*_\alpha$ of this elliptic boundary value problem implicitly defines the induced strain $\boldsymbol{\varepsilon}^*_\alpha$ and stress field $\boldsymbol{\sigma}^*_\alpha$. Introducing the elastic localization operators $\mathbb{Y}$ for the displacement field and $\mathbb{A}$ for the strain field, the local stress, strain and displacement fields

$$\boldsymbol{u} = \mathbb{Y}[\bar{\boldsymbol{\varepsilon}}] + \sum_{\alpha=1}^{N} \xi_\alpha \boldsymbol{u}^*_\alpha, \qquad \boldsymbol{\varepsilon} = \mathbb{A}[\bar{\boldsymbol{\varepsilon}}] + \sum_{\alpha=1}^{N} \xi_\alpha \boldsymbol{\varepsilon}^*_\alpha, \qquad \boldsymbol{\sigma} = \mathbb{C}\mathbb{A}[\bar{\boldsymbol{\varepsilon}}] + \sum_{\alpha=1}^{N} \xi_\alpha \boldsymbol{\sigma}^*_\alpha \tag{14}$$

solve the microscopic balance of linear momentum for arbitrary (but given) mode stimulation coefficients ξ_α. In order to determine the evolution of the latter, the thermodynamic conjugated forces

$$\tau_\alpha = \langle \mathbb{A}^{\mathsf{T}}\mathbb{C}[\boldsymbol{\mu}_\alpha] \rangle \cdot \bar{\boldsymbol{\varepsilon}} + \sum_{\beta=1}^{N} \xi_\beta \langle \boldsymbol{\sigma}^*_\beta \cdot \boldsymbol{\mu}_\alpha \rangle \tag{15}$$

are introduced. All conjugate forces τ_α are assembled into the N-dimensional vector $\hat{\tau}$. The following investigations are based on the coupled model of Michel and Suquet (2003, 2004). The matrix material in which the particles are embedded into is assumed to be aluminum with the properties reported by Michel and Suquet (2003) and the ceramic particles are assumed elastic with the material properties of SiC particles according to Chawla et al. (2006) (Tab. 2). The non-linear isotropic hardening of the metal phase is described in terms of a von Mises-type yield criterion with the yield stress

$$\sigma_{\mathrm{F}}(\bar{q}) = \sigma_0 + h\bar{q}^l, \tag{16}$$

where $\bar{q}$ an effective hardening variable resembling the accumulated plastic strain. Following the hypothesis (H1) introduced by Michel and Suquet (2003) the effective internal variable $\bar{q}$ is assumed constant over the unit cell. The elastic and inelastic parameters of the matrix material and of the ceramic particles are characteristic for the considered class of particulate metal matrix composites in general and are hence chosen in the current investigation.

	E	ν	σ_0	h	l
Aluminum	75 GPa	0.33	75 MPa	416.5 MPa	0.3895
SiC particles	400 GPa	0.19	-	-	-

Table 2: Material parameters for an Al/SiC_p-type composites cf. Michel and Suquet (2003); Chawla et al. (2006)

According to Fritzen and Böhlke (2010c), the evolution of the internal variables is described by the effective yield function

$$\bar{\varphi}(\hat{\tau}) = \|\hat{\tau}\|_2 - \sqrt{2/3}\, c\, \sigma_{\mathrm{F}}(\bar{q}), \tag{17}$$

where c is the volume fraction of the inelastic material. Then the rates for $\hat{\xi}$ and $\bar{q}$ are determined by

$$\bar{\varphi} \leq 0, \qquad \dot{\gamma} \geq 0, \qquad \dot{\gamma}\bar{\varphi} = 0, \qquad \dot{\hat{\xi}} = \dot{\gamma}\frac{\partial \bar{\varphi}}{\partial \hat{\tau}}, \qquad \dot{\bar{q}} = \sqrt{\frac{2}{3}}\dot{\gamma}. \tag{18}$$

Details concerning the various data processing steps needed to implement the non-uniform transformation field analysis have extensively been described by Fritzen and Böhlke (2010c). Note that based on (14) and with the effective linear elastic operator $\bar{\mathbb{C}}$, the macroscopic stress is a linear transformation of the macroscopic strain $\bar{\boldsymbol{\varepsilon}}$ and the vector of mode activity coefficients $\hat{\xi}$

$$\bar{\boldsymbol{\sigma}} = \bar{\mathbb{C}}[\bar{\boldsymbol{\varepsilon}}] + \sum_{\alpha=1}^{N} \langle \boldsymbol{\sigma}_*^{(\alpha)} \rangle \xi_\alpha. \tag{19}$$

4. Numerical results

4.1. Oblate particles

4.1.1. Elastic properties

First, the elastic anisotropy of the material with oblate microstructure is investigated. Therefore, the effective stiffness tensor $\bar{\mathbb{C}}$ of the material is determined. A graphical representation for the directional dependency of the Young's modulus is given by (see, e.g., Böhlke and Brüggemann, 2001)

$$E(\boldsymbol{n}) = \frac{1}{\boldsymbol{n} \otimes \boldsymbol{n} \cdot \bar{\mathbb{C}}^{-1}[\boldsymbol{n} \otimes \boldsymbol{n}]}, \tag{20}$$

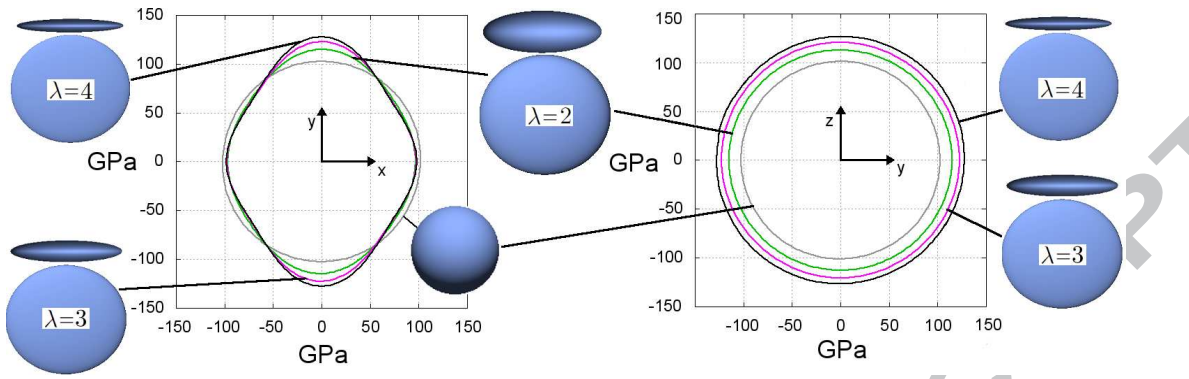

Fig. 8: Representation of the directional Young's modulus $E(\boldsymbol{n})$ in the x-y plane (left) and in the y-z-plane (transverse plane; right) for oblate particle reinforced metal matrix composites for $\lambda = 2, 3, 4$ compared to the Young's modulus of the isotropic microstructure (grey circle)

where $\boldsymbol{n}$ denotes a unit normal vector. The results are shown in Fig. 8 for the x-y-plane (left) and the y-z-plane (transverse direction, right). The idealized particle shapes associated with the microstructures are also shown.

Surprisingly, the Young's modulus in the x-direction decreases by only 7.3% for the flattest particle ($\lambda = 4$) when compared to the isotropic particle system. However, the directional Young's modulus in the transverse direction increases by approximately 24.2% relative to the isotropic ensemble for the same microstructure. Additionally, it is found that the Young's modulus in the transverse plane is isotropic up to an in-plane deviation of 1.33% for these particles. Hence, the considered unit cell can be considered statistically representative. If the morphological anisotropy is chosen smaller, the results scale between the ones obtained with an isotropic morphology and the one for $\lambda = 4$ (see Fig. 8).

4.1.2. Comparison to full-field simulations

In order to identify the inelastic modes a series of five ortho-normal deviatoric strain loadings was prescribed to each unit cell model. At each load increment with index α the plastic strain field $\boldsymbol{\varepsilon}^{\mathrm{p}}_{\alpha}$ was stored. Then the covariance matrix

$$S_{\alpha\beta} = \langle \boldsymbol{\varepsilon}^{\mathrm{p}}_{\alpha} \cdot \boldsymbol{\varepsilon}^{\mathrm{p}}_{\beta} \rangle_{\Omega_{\mathrm{p}}} \tag{21}$$

was evaluated and the largest eigenvalues up to a relative discrepancy of 10^{-5} with respect to the largest identified value were taken to construct the modes following the proposition of Roussette et al. (2009). Finally, the modes are renormalized. The number of inelastic modes thereby identified was twelve ($\lambda = 2$) and thirteen ($\lambda = 3, 4$) for the three considered microstructures containing oblate particles. For a detailed description of the implementation of the computational steps involved in the method we refer to Fritzen and Böhlke (2010c), where a first application of the NTFA to three-dimensional problems was published. Note that different loadings could have equally been chosen, such as anti-periodic traction fluctuation boundary conditions.

The particular focus of this paper is the investigation of the presumable anisotropic inelastic constitutive behavior of composites with morphological anisotropy using the NTFA. So far, only near

isotropic inclusions have been considered for the use with the NTFA, and it was shown that the method performs well for these microstructures. In order to validate the homogenized material law for anisotropic micro-morphologies, the two proportional strain paths

$$\dot{\bar{\boldsymbol{\varepsilon}}}_1 = 1\,\mathrm{s}^{-1} \begin{pmatrix} 0.0169 & -0.0405 & -0.0053 \\ & -0.0159 & -0.0103 \\ \text{sym.} & & 0.0392 \end{pmatrix} \boldsymbol{e}_i \otimes \boldsymbol{e}_j \tag{22}$$

$$\dot{\bar{\boldsymbol{\varepsilon}}}_2 = 1\,\mathrm{s}^{-1} \begin{pmatrix} 0.0361 & -0.0014 & -0.0074 \\ & 0.0401 & 0.0199 \\ \text{sym.} & & -0.0426 \end{pmatrix} \boldsymbol{e}_i \otimes \boldsymbol{e}_j \tag{23}$$

are imposed on both, the unit cell in a full-field simulation and the homogenized material model. The amplitude was normalized to give a total loading of $\|\bar{\boldsymbol{\varepsilon}}_i(t_{\max})\|_2 = 7.5\%$. Both loading directions are generated using random numbers and it was verified that the correlation of the considered loading to the loading paths used in the mode identification process is negligible.

The verification has been carried out for all $\lambda \in \{2, 3, 4\}$ in both loading directions. The maximum relative errors δ with respect to the virtual process time

$$\delta = \max_t \left(\frac{\|\bar{\boldsymbol{\sigma}}_{\mathrm{NTFA}}(t) - \bar{\boldsymbol{\sigma}}_{\mathrm{FEM}}(t)\|_2}{\|\bar{\boldsymbol{\sigma}}_{\mathrm{FEM}}(t)\|_2} \right) \tag{24}$$

are summarized in Tab. 3 for the oblate particle shapes.

microstructure	δ for $\dot{\bar{\boldsymbol{\varepsilon}}} = \dot{\bar{\boldsymbol{\varepsilon}}}_1$ [%]	δ for $\dot{\bar{\boldsymbol{\varepsilon}}} = \dot{\bar{\boldsymbol{\varepsilon}}}_2$ [%]
oblate, $\lambda = 2$	4.663 %	4.622%
oblate, $\lambda = 3$	3.884 %	3.907 %
oblate, $\lambda = 4$	2.957 %	2.913 %

Table 3: Relative errors of the NTFA versus full-field simulations for the oblate particles ($\lambda = 2, 3, 4$)

In order to visualize the good agreement of the two approaches, the components of the effective stress tensor of the homogenized model and the full-field simulation are plotted in Fig. 9 for two different microstructures and the two different loadings with respect to the process time (left: $\lambda = 2$, $\dot{\bar{\boldsymbol{\varepsilon}}}_2$, right: $\lambda = 3$, $\dot{\bar{\boldsymbol{\varepsilon}}}_1$).

4.1.3. Computational efficiency

The computational effort to solve the periodic full-field problem on cuboidal unit cells is generally a challenging procedure. The linear system of equations obtained from the finite element analysis has a prohibitively large bandwidth due to the linear relation of the degrees of freedom on opposing sides of the unit cell. The latter leads to tremendous amounts of fill-in during a direct

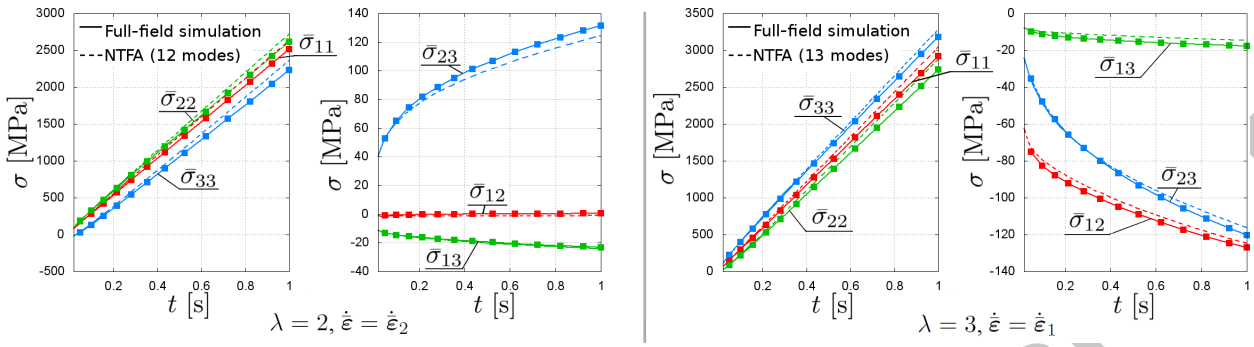

Fig. 9: Comparison of the components of the homogenized stress tensor between full-field simulation and NTFA model for the oblate microstructure (left: $\lambda = 2, \dot{\bar{\varepsilon}} = \dot{\bar{\varepsilon}}_2$, 12 modes; right: $\lambda = 3, \dot{\bar{\varepsilon}} = \dot{\bar{\varepsilon}}_1$, 13 modes)

solution step using state-of-the-art direct solvers such as MUMPS, PARDISO or DSCPACK. Although the mandatory graph-based reordering strategies relying on METIS or SCOTCH can reduce the amount of fill-in significantly, the amount of memory required is still prohibitively large. For the strong morphological contrasts considered here, the number of surface nodes subjected to linear equation constraints is considerably increased over a cubic unit cell. More specifically, the use of desktop computers is not possible due to memory requirements easily depassing the 8GB limit. Additionally, the computational time is also significant. The previously described implications due to the type of boundary condition are addressed in Fritzen and Böhlke (2010a).

In order to reduce both, the memory and cpu time required, a preconditioned conjugate gradient method is used based on an incomplete LU factorization (here: incomplete cholesky) developed by Bollhoefer and Saad (2006). In the considered numerical examples, the maximum memory requirement was less than three GB in the preconditioning phase and eight hundred MB in the iteration process. The solution time for the linear systems of the finite element analysis containing 400000 degrees of freedom ranged between two and eight minutes using a single CPU. The total solution time for an entire strain path computation ranged between two and four hours and produced approximately one GB of binary data. These values outline the capability of the iterative solving technique to allow for representative computations on standard hardware. The total input data for the seven different microstructures (isotropic, 3×oblate, 3×elongated) and the considered seven different strain paths (five for the mode identification, two for the validation) resulted in a total data volume of 45 GB and a solution time of approximately one week on a single workstation. Taking this storage requirement and the CPU time into account the authors presume that FE^2 type approaches (Feyel, 1998) with sufficiently fine spatial discretization will not make their way into three-dimensional real world problems in the near future.

4.2. Elongated particles

4.2.1. Elastic properties

Analogous to the oblate particles, the elastic properties of micro-heterogeneous materials containing elongated particles are examined. The directional Young's modulus $E(\boldsymbol{n})$ is compared to the

one of the isotropic comparison structure in Fig. 10. The directional stiffening of the elongated particles for $\lambda = 4$ in x-direction is 30.1% with respect to the isotropic microstructure, while the smallest directional Young's modulus is decreased by 3%. Again, almost perfect transverse isotropy was found with the largest in-plane deviation being 1.45%. The ratio of the largest and smallest observed directional stiffness was 1.361 for the elongated particles and 1.364 for the oblate particles.

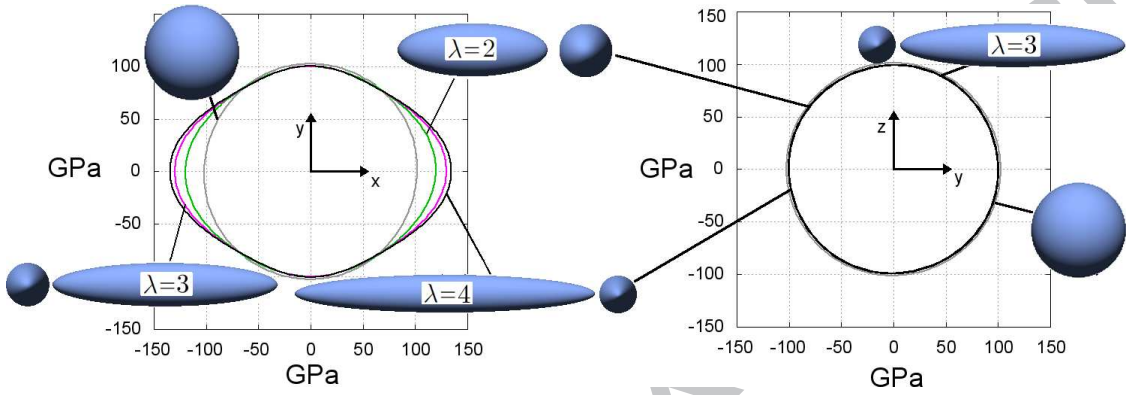

Fig. 10: Representation of the directional Young's modulus $E(\boldsymbol{n})$ in the x-y plane (left) and in the y-z-plane (transverse direction; right) for elongated particle reinforced metal matrix composites for $\lambda = 2, 3, 4$ compared to the Young's modulus of the isotropic microstructure (grey circle)

4.2.2. Comparison to full-field simulations

The NTFA was applied to the three different microstructures containing elongated particles and 12 ($\lambda = 2$) and 11 ($\lambda = 3, 4$) inelastic modes were identified. The same identification procedure as for the oblate particles was used. The same numerical verification procedure based on the random loadings (22), (23) was performed to validate the NTFA for further use. The components of the macroscopic stress tensor for two of the six validation computations are presented in Fig. 11 for the full-field simulation and the NTFA (dashed line). In addition, the relative errors for all computations are provided in Tab. 4.

microstructure	δ for $\dot{\bar{\varepsilon}} = \dot{\bar{\varepsilon}}_1$ [%]	δ for $\dot{\bar{\varepsilon}} = \dot{\bar{\varepsilon}}_2$ [%]
elongated, $\lambda = 2$	5.657 %	9.445 %
elongated, $\lambda = 3$	4.252 %	4.015 %
elongated, $\lambda = 4$	3.584 %	3.362%

Table 4: Relative errors of the NTFA versus full-field simulations for the elongated particles ($\lambda = 2, 3, 4$)

Similarly to the oblate particles a good agreement between full-field simulation and reduced model could be observed for all examined anisotropy ratios and for all loading directions.

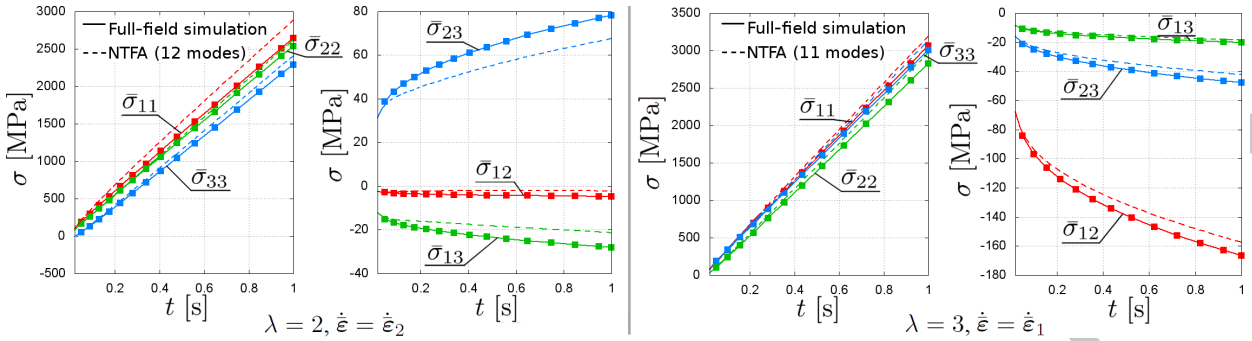

Fig. 11: Comparison of the components of the homogenized stress tensor between full-field simulation and NTFA model for the elongated microstructure (left: $\lambda = 2$, $\dot{\bar{\varepsilon}} = \dot{\bar{\varepsilon}}_2$, 12 modes; right: $\lambda = 3$, $\dot{\bar{\varepsilon}} = \dot{\bar{\varepsilon}}_1$, 11 modes)

4.3. Load transfer

While the homogenized stress is of ultimate interest for structural computations, the load partitioning between the matrix material and the reinforcement is an important indicator for the efficiency of the material. Moreover, an approximation of the load partitioning can be measured in experiments using x-ray diffraction methods. In these experiments the material parameters of all components are assumed isotropic and the crystallographic orientation is assumed isotropic throughout the investigated cross-section. In particular, the method provides an estimate of the average uni-axial phase-stress in each constituent of a specimen subjected to a uni-axial loading. In the following a method for the description of the load partitioning for three-dimensional macroscopic stress states $\bar{\boldsymbol{\sigma}}$ is introduced. Therefore, the average stress tensors in the individual phases

$$\bar{\boldsymbol{\sigma}}_i = \langle \boldsymbol{\sigma} \rangle_{\Omega_i} \tag{25}$$

are computed. The effective stress tensor for a N-component material can then be decomposed according to

$$\bar{\boldsymbol{\sigma}} = \sum_{i=1}^{N} c_i \bar{\boldsymbol{\sigma}}_i, \tag{26}$$

where c_i is the volume fraction of the i-th material. We define the load partition ϕ_i contributed by the i-th material by the projection

$$\phi_i = \frac{c_i \bar{\boldsymbol{\sigma}}_i \cdot \bar{\boldsymbol{\sigma}}}{\bar{\boldsymbol{\sigma}} \cdot \bar{\boldsymbol{\sigma}}}. \tag{27}$$

Note that the sum of all load fractions yields 100%, i.e.,

$$1 = \sum_{i=1}^{N} \phi_i. \tag{28}$$

In the following the index i is omitted and the reported load fractions refer to the metallic constituent. The numerical values of ϕ have been evaluated based on the NTFA approach and based

on the full-field simulations. The results are compared for the oblate particles (Fig. 12) and the elongated particles (Fig. 13) and for the three loadings

$$\dot{\bar{\varepsilon}}_3 = (2\boldsymbol{e}_1 \otimes \boldsymbol{e}_1 - \boldsymbol{e}_2 \otimes \boldsymbol{e}_2 - \boldsymbol{e}_3 \otimes \boldsymbol{e}_3)\frac{0.15}{\mathrm{s}}, \tag{29}$$

$$\dot{\bar{\varepsilon}}_4 = (\boldsymbol{e}_1 \otimes \boldsymbol{e}_2 + \boldsymbol{e}_2 \otimes \boldsymbol{e}_1)\frac{0.15}{\mathrm{s}}, \tag{30}$$

$$\dot{\bar{\varepsilon}}_5 = (\boldsymbol{e}_1 \otimes \boldsymbol{e}_3 + \boldsymbol{e}_3 \otimes \boldsymbol{e}_1)\frac{0.15}{\mathrm{s}}. \tag{31}$$

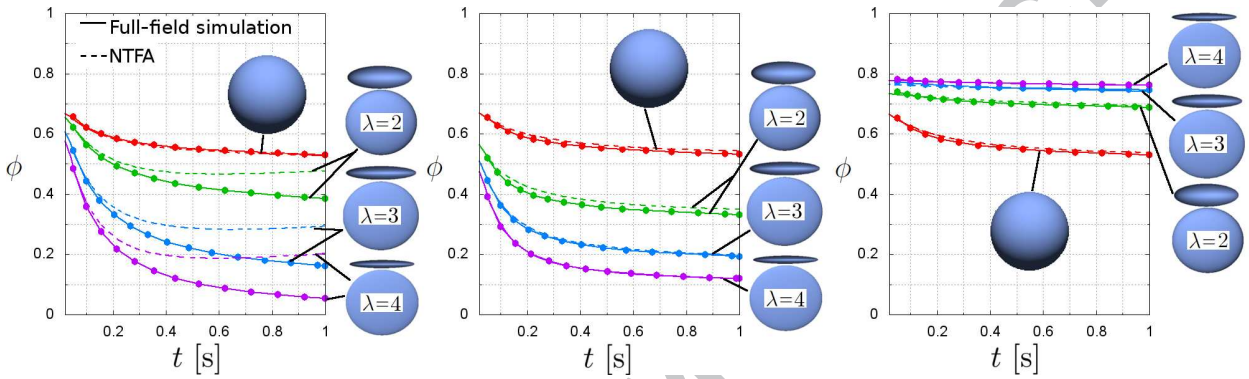

Fig. 12: Comparison of the load fraction ϕ of the metal matrix for the macroscopic loadings $\dot{\bar{\varepsilon}}_3$ (left) $\dot{\bar{\varepsilon}}_4$ (middle) and $\dot{\bar{\varepsilon}}_5$ (right) for the oblate microstructures; for comparison the values of the isotropic structure are also shown (red curves)

The loadings represent isochoric tension in the direction of the elongation/compression, shear in the plane spanned by the particle principle axis and the y-direction and shear in the transverse plane (y-z-plane). The results state a good qualitative agreement between the NTFA model and the full-field simulation. However, a quantitative discrepancy was observed for the isochoric tension.

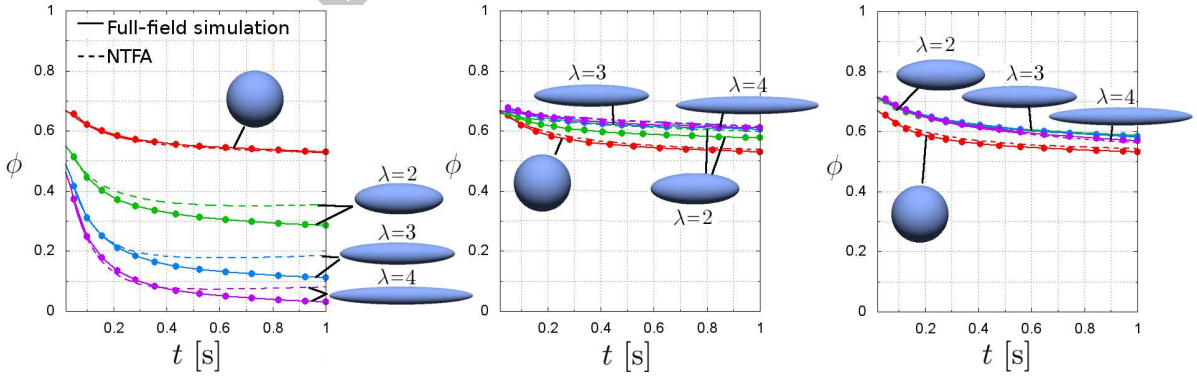

Fig. 13: Comparison of the load fraction ϕ of the metal matrix for the macroscopic loadings $\dot{\bar{\varepsilon}}_3$ (left) $\dot{\bar{\varepsilon}}_4$ (middle) and $\dot{\bar{\varepsilon}}_5$ (right) for the elongated microstructures; for comparison the values of the isotropic structure are also shown (red curves)

A fundamentally different change in the load transfer behavior was observed during proportional loading for the various examined microstructures. Taking into account that the load fraction carried

by the particles is

$$\phi_{\mathrm{p}} = 1 - \phi, \tag{32}$$

it can be concluded from the leftmost graph in Fig. 12 and 13 that the anisotropic particle shape leads to a significant decrease of the load carried by the matrix, i.e. the load is transferred to the particles. The load transfer is more pronounced for the elongated particles in both, the NTFA and the full-field simulation. Regarding shear in the x-y plane (Fig. 12, 13, middle), the oblate particles show a completely different load transfer behavior than the elongated and the isotropic structure. More precisely, the higher the morphological anisotropy ratio λ, the more load is transferred to the particles, whereas the elongated particles show almost an identical load transfer behavior as the isotropic microstructures.

5. Summary and conclusions

5.1. Summary

A novel method for the generation of anisotropic periodic particle systems is presented in section 2. Based on recent mesh generation techniques developed by the authors (Fritzen et al., 2009; Fritzen and Böhlke, 2010b), the examined microstructures are discretized, resulting in a periodic high quality finite element mesh. Two important morphological classes are investigated: oblate particles which are representative for many whisker reinforced materials and elongated particles aiming at short fiber reinforced materials. Additionally, different amounts of anisotropy are considered in terms of three different values of the elongation parameter λ. The ability of the method to reproduce some of the statistical properties of real Al-SiC composites investigated by Ganesh and Chawla (2005) is demonstrated. Some statistical properties of the reinforcement such as the aspect ratio and the orientation of the principle particle axis are discussed. The particle volume fraction in all investigations is 20 % which is an appropriate value for many real world materials.

The theory of the non-uniform transformation field analysis is briefly reviewed in 3 (see Fritzen and Böhlke (2010c) for details) and the method is applied to the generated model microstructures in 4. First, the elastic anisotropy is evaluated and it is found that the ratio of the highest to lowest directional Young's modulus is almost identical for the oblate and the elongated microstructure, if the value λ is the same for both. While the oblate particles lead to stiffening in the transverse plane, the needle shaped particles result in a more pronounced elastic stiffening in direction of the elongation axis.

The inelastic material response of the homogenized material model is compared to full-field simulations. A good qualitative and quantitative agreement of the reduced model with the fully resolved computations was found. Notably, only a hand full of mode stimulation coefficients are needed for the reduced model while the full-field model involves several hundred thousand unknown nodal displacements plus the inelastic variables at each integration point. The computational cost is hard to quantify since the reduced model requires only a few milliseconds for a

full strain path computation. The same numerical experiment (with a smaller number of time increments) requires several hours of CPU time when performed in terms of a full-field simulation.

Additionally, the load partitioning between the reinforcement and the matrix material is examined in 4.3. It is found that the NTFA can capture the load partitioning quite well despite some quantitative discrepancy. The load transfer behavior of the anisotropic microstructures is found to strongly differ from the one observed for statistically isotropic particles.

5.2. Conclusions

The NTFA is applied to three-dimensional microstructured materials with pronounced anisotropic morphology. To our knowledge this is the first application of the method to three-dimensional problems with geometric anisotropy and one of the first applications to three-dimensional problems in general. The presented results show a good agreement between full-field simulations and the reduced homogenized material model despite the strong morphological heterogeneity. While the macroscopic stress response is well described by the reduced model, a speed-up of more than 10^6 is observed over the full-field simulations.

The authors would like to point out that the NTFA does not require additional fitting parameters or a posteriori adjustments required by many phenomenological approaches. Provided the microstructural constitutive behavior is well known, all coefficients entering in the formulation of the homogenized material response are solely depending on a micromechanical analysis. The latter is carried out in terms of a hand-full of numerical simulations on a fully resolved microstructure and the results of these computations are no longer needed, once the modes are identified. Hence, an entire database of material parameters for various microstructures can be created with negligible storage requirements.

The evaluation of the load partitioning is a useful tool for real world applications of composite materials. The method allows to evaluate the effect of non-uniform microstructural morphology on the response of large scale structures, e.g., the effect of locally anisotropic particles near macroscopic geometric features. Moreover, the design of structures with optimal microstructure is possible by varying (locally) the amount of anisotropy and/or the orientation of the composite. Investigations exploring these aspects further are planned.

References

References

Barber, C., Dobkin, D., Huhdanpaa, H., 1996. The Quickhull algorithm for convex hulls. ACM Trans. Math. Softw. 22, 469–483.

Böhlke, T., Brüggemann, C., 2001. Graphical representation of the generalized hooke's law. TECHNISCHE MECHANIK 21, 145–158.

Böhlke, T., Jöchen, K., Kraft, O., Löhe, D., Schulze, V., 2010. Elastic properties of polycrystalline microcomponents. Mechanics of Materials 42, 11–23.

Bollhoefer, M., Saad, Y., 2006. Multilevel preconditioners constructed from inverse-based ilus. SIAM J. Sci. Comput., Special Issue on the 8-th Copper Mountain Conference 5, 1627–1650.

REFERENCES

Carrere, N., Feyel, F., Kruch, S., 2003. Multi-scale modelling of silicon carbide reinforced titanium mmcs: Application to advanced compressor design. Aerospace Science and Technology 7, 307 – 315.

Chaboche, J., Kanouté, P., Roos, A., 2005. On the capabilities of mean-field approaches for the description of plasticity in metal matrix composites. International Journal of Plasticity 21, 1409 – 1434.

Chawla, N., Deng, X., Schnell, D., 2006. Thermal expansion anisotropy in extruded SiC particle reinforced 2080 aluminum alloy matrix composites. Materials Science and Engineering A 426, 314–322.

Doghri, I., Ouaar, A., 2003. Homogenization of two-phase elasto-plastic composite materials and structures study of tangent operators, cyclic plasticity and numerical algorithms. International Journal of Solids and Structures 40, 1681–1712.

Du, Q., Faber, V., Gunzburger, M., 1999. Centroidal Voronoi Tessellations: Applications and Algorithms. SIAM Review 41, 637–676.

Dvorak, G., Bahei-El-Din, Y., Wafa, A., 1994a. Implementation of the transformation field analysis. Computational Mechanics 14 , 201–228.

Dvorak, G., Bahei-El-Din, Y., Wafa, A., 1994b. The modeling of inelastic composite materials with the transformation field analysis. Modelling and Simulation in Material Science and Engineering 2, 571–586.

Dvorak, G., Benveniste, Y., 1992. On transformation strains and uniform fields in multiphase elastic media. Proceedings of the Royal Society of London A , 291–310.

Dvorak, G.J., Zhang, J., 2001. Transformation field analysis of damage evolution in composite materials. Journal of the Mechanics and Physics of Solids 49, 2517 – 2541.

Feyel, F., 1998. Application du calcul parallèle aux modèles à grand nombre de variables internes. Ph.D. thesis. Ecole National Supérieure des Mines de Paris.

Flaquer, J., Ríos, A., Martín-Meizoso, A., Nogales, S., Böhm, H., 2007. Effect of diamond shapes and associated thermal boundary resistance on thermal conductivity of diamond-based composites. Computational Materials Science 41, 156 – 163.

Fritzen, F., Böhlke, T., 2010a. Influence of the type of boundary conditions on the numerical properties of unit cell problems. Technische Mechanik 30, 354–363.

Fritzen, F., Böhlke, T., 2010b. Periodic three-dimensional mesh generation for particle reinforced composites with application to metal matrix composites. International Journal of Solids and Structures accepted for publication.

Fritzen, F., Böhlke, T., 2010c. Three-dimensional finite element implementation of the nonuniform transformation field analysis. International Journal for Numerical Methods in Engineering 84, 803–829.

Fritzen, F., Böhlke, T., 2009a. Homogenization of the physically nonlinear properties of three-dimensional metal matrix composites using the nonuniform transformation field analysis, pp. 1–10.

Fritzen, F., Böhlke, T., 2009b. Homogenization of three-dimensional micro-heterogeneous materials using nonuniform transformation fields, pp. 1–12.

Fritzen, F., Böhlke, T., Schnack, E., 2009. Periodic three-dimensional mesh generation for crystalline aggregates based on voronoi tessellations. Computational Mechanics 43, 701–713.

Ganesh, V., Chawla, N., 2005. Effect of particle orientation anisotropy on the tensile behavior of metal matrix composites: experiments and microstructure-based simulation. Materials Science and Engineering A 391, 342–353.

Ghosh, S., Lee, K., Moorthy, S., 1995. Multiple scale analysis of heterogeneous elastic structures using homogenization theory and voronoi cell finite element method. International Journal of Solids and Structures 32, 27 – 62.

Ghosh, S., Lee, K., Moorthy, S., 1996. Two scale analysis of heterogeneous elastic-plastic materials with asymptotic homogenization and voronoi cell finite element model. Computer Methods in Applied Mechanics and Engineering 132, 63 – 116.

Halphen, N., Nguyen, Q., 1975. Sur les matériaux standards generalisés. J. Méc. , 508–520.

Hashin, Z., Shtrikman, S., 1962. A variational approach to the theory of the elastic behaviour of polycrystals. Journal of the Mechanics and Physics of Solids 10, 343–352.

Jöchen, K., Böhlke, T., Fritzen, F., 2010. Influence of the crystallographic and the morphological texture on the elastic properties of fcc crystal aggregates. Solid State Phenomena 160, 83–86.

Kanoute, P., Boso, D., Chaboche, J., Schrefler, B., 2009. Multiscale Methods For Composites: A Review. Archives

of Computational Methods in Engineering 16, 31–75.

Kröner, E., 1958. Berechnung der elastischen Konstanten des Vielkristalls aus den Konstanten des Einkristalls. Z. Phys. 151, 504–518.

Michel, J., Suquet, P., 2003. Nonuniform transformation field analysis. International Journal of Solids and Structures 40, 6937–6955.

Michel, J., Suquet, P., 2004. Computational analysis of nonlinear composite structures using the nonuniform transformation field analysis. Computer Methods in Applied Mechanics and Engineering 193, 5477–5502.

Michel, J.C., Suquet, P., 2009. Nonuniform transformation field analysis: a reduced model for multiscale nonlinear problems in solid mechanics, in: Galvanetto, U., Aliabadi, F. (Eds.), Multiscale Modelling in Solid Mechanics - Computational Approaches. Imperial College Press, London.. Imperial College Press, pp. 159–206. ISBN: 978-1-84816-307-2. OR 1.

Miracle, D., 2005. Metal matrix composites - from science to technological significance. Composites Science and Technology 65, 2526–2540.

Mori, T., Tanaka, K., 1973. Average Stress in A Matrix and Average Elastic Energy of Materials with Misfitting Inclusions. Acta Metallurgica et Materialia 23, 571–574.

Oskay, C., Fish, J., 2007. Eigendeformation-based reduced order homogenization for failure analysis of heterogeneous materials. Computer Methods in Applied Mechanics and Engineering 196, 1216 – 1243.

Reuss, A., 1929. Berechnung der fließgrenze von mischkristallen auf grund der plastizitätsbedingung für einkristalle. Zeitschrift für Angewandte Mathematik und Mechanik 9, 49–58.

Roussette, S., Michel, J., Suquet, P., 2009. Nonuniform transformation field analysis of elastic-viscoplastic composites. Composite Science and Technology 69, 22–27.

Shewchuk, J., 1996. Engineering a 2D Quality Mesh Generator and Delaunay Triangulator, in: Lin, M., Manocha, D. (Eds.), Applied Computational Geometry: Towards Geometric Engineering. Springer-Verlag, pp. 203–222.

Si, H., Gaertner, K., 2005. Meshing Piecewise Linear Complexes by Constrained Delaunay Tetrahedralizations, in: Proceedings of the 14th International Meshing Roundtable, pp. 147–163.

Suquet, P., 1985. Local and global aspects in the mathematical theory of plasticity. Elsevier, London. Plasticity Today: Modelling, Methods and Applications, pp. 279–310.

Suresh, S. (Ed.), 2002. Fundamentals of metal matrix composites. Knovel, Norwich, NY.

Voigt, W., 1910. Teubner, Berlin. Lehrbuch der Kristallphysik.

Willis, J., 1977. Bounds and self-consistent estimates for the overall properties of anisotropic composites. Journal of the Mechanics and Physics of Solids 25, 185–202.

Willis, J., 1981. Variational and related methods for the overall properties of composites, Elsevier. volume 21 of *Advances in Applied Mechanics*, pp. 1–78.